Hydrol. Earth Syst. Sci. Discuss., 12, 2497–2525, 2015
www.hydrol-earth-syst-sci-discuss.net/12/2497/2015/
doi:10.5194/hessd-12-2497-2015

Hydrology and Earth System Sciences
Open Access
Discussions

Simulating the regional water balance through hydrological model based on TRMM satellite rainfall data

D. Li[1], X. Ding[2], and J. Wu[3]

[1]College of Environmental and Resource Sciences, Zhejiang University, Hangzhou, China
[2]Laohutan Reservoir management office of Huzhou City, Huzhou, China
[3]Ocean College, Zhejiang University, Hangzhou, China

Received: 2 February 2015 – Accepted: 2 February 2015 – Published: 27 February 2015

Correspondence to: J. Wu (jw67@zju.edu.cn)

Published by Copernicus Publications on behalf of the European Geosciences Union.

Abstract

Spatial rainfall is a key input to Distributed Hydrological Models, which is the most important limitation for the accuracy of hydrological models. Model performance and uncertainty could increase when rain gauge is sparse. Satellite-based precipitation products would be an alternative to ground-based rainfall estimates in present and the foreseeable future, however, it is necessary to evaluate the products before further implication. The objective of this paper is to provide assessments of: (a) the Tropical Rainfall Measuring Mission (TRMM) rainfall product using gauge data, (b) the TRMM rainfall as forcing data for hydrological simulation, and (c) the role of satellite data in calculating water balance and water management. TRMM rainfall data show reasonable performances at monthly and annual scales, fitting well with surface observation-based histogram of precipitation. Satisfactory performances in monthly runoff simulation (NS = 0.50 ~ 0.70, R^2 = 0.73 ~ 0.85) observed in our study indicate that the TRMM rainfall data have potential applications in driving hydrological model, water balance analysis, and basin water resource management in developing countries or remote locations, where precipitation gauges are scare.

1 Introduction

Precipitation is widely accepted as a fundamental component of the global water cycle and in a sense governs the renewable water resources that affect economic, ecological and agricultural development. The spatial and temporal resolutions of precipitation data are mutually influenced, and both have significant impacts on determining surface hydrology (Masih et al., 2011; Michaelides et al., 2009; Xu et al., 2013). As hydrological models are abstract and simplified representations of natural hydrological processes, those models well founded in physical theory and empirically justified by past performance. However, those models will fail to produce accurate hydrograph predictions if the precisions of inputting precipitation data are not high enough.

HESSD
12, 2497–2525, 2015

In general, precipitation gauges provide the primary means of estimating precipitation at a point, and calculated regional precipitation by interpolation methods such as Kriging, Thiessen polygons and Trend surface analysis. It is commonly believed that the areas of high rain gauge density can provide more reliable estimates at an unsampled location than that of low rain gauge density (Chappell et al., 2013). However, in some places the ground-based observations are usually sparse or unevenly distributed due to economic or terrain limitation. Furthermore, rain gauge observations are usually not available in real time in many regions.

The estimation of the spatial distribution of rainfall can be improved with the inclusion of ancillary data such as radar, satellite and topography. Moreno et al. (2012) revealed that radar and multisensor quantitative precipitation estimates lead to improving hydrologic model performance compared to simulations driven with rain gauge data only. Hunink et al. (2014) found that blending satellite rainfall products with altitude and vegetation index would continuously improve quantification the spatial distribution of precipitation. In addition, high resolution satellite rainfall estimates was used in quite a lot of studies as a source of data for hydrological application and water resources planning (Masih et al., 2011; Ud din et al., 2008; Wilk et al., 2006; Yan and Gebremichael, 2009; Zhang et al., 2009). As a result, satellite rainfall estimates open novel avenues for forecasting in regions with limited access and sparse observations (Moreno et al., 2012).

Since the launch of the Tropical Rainfall Measuring Mission (TRMM; Kummerow, 1998) in 1997, the first precipitation radar sensor stared to be operated in space. The availability of active precipitation detection from space has laid the groundwork for spaceborne estimations from radar and radar + radiometer (Michaelides et al., 2009). However, the absolute accuracy of satellite rainfall products is questionable (Tian and Peters-Lidard, 2010), and needs a thorough validation before it can be used extensively.

Recently, many studies evaluated the performance of satellite rainfall products over different regions in the world (Dinku et al., 2008; Hu et al., 2013; Jiang et al., 2010; Li

HESSD
12, 2497–2525, 2015

et al., 2012; Ochoa et al., 2014; Shen et al., 2010; Stampoulis and Anagnostou, 2012; Worqlul et al., 2014).The results of these studies indicated that the quality of satellite rainfall products varies with season, region, and elevation. Basically, the TRMM 3B42 product performs reasonably well over most regions in depicting the overall rainfall spatial patterns with only small biases compared to the gauge data. But the TRMM 3B42 generally underestimates rainfall over higher elevations, especially during the cold season. However, fewer studies compare TRMM rainfall data and rain gauge data at catchment scale, and fewer evaluation of hydrological processes using TRMM rainfall data in simulation and water balance analysis in catchments scale, which will provide useful information for hydrology research and water management.

This study is aimed at: (1) evaluate the accuracy of TRMM rainfall product by using a hydrologic model to calculate runoff and compare to measured runoff, (2) evaluate the suitability of TRMM rainfall product used for simulating regional water balance. Section 2 of this paper provides a brief introduction of the focus region of this study, along with a brief discussion on the rain gauge and TRMM rainfall data. Section 3 first presents the performance of TRMM rainfall to the rain gauge data, then processes the hydrological simulation driven by two types of rainfall, and finally describes the water balance of the watershed.

2 Study area and data description

2.1 Study area

The Tiaoxi watershed with an area of 5900 km^2 is situated in eastern China, which is a part of southern catchment of Taihu Lake (Fig. 1). It is located at 119°13′–120°19′ E longitude and 30°7′–31°11′ N latitude. The Tiaoxi River is the major tributary of Taihu Lake basin, supplying drinking water for 8 million residents in Hangzhou and Huzhou. The mean sea level of this area varies from 3 to 1571 m, with alluvial plains lying in the northeastern parts. The whole watershed is characterized by a semitropical cli-

HESSD
12, 2497–2525, 2015

mate with an average annual temperature and precipitation of 15.6 °C and 1460 mm, respectively.

Department of Water Resources of Zhejiang Province measured discharge of several gauging stations at Tiaoxi watershed. The measured daily flow data at the "Gangkou" and "Pingyao" gauging stations during 1999–2008 was collected and used in the present study. The drainage area represented by Gangkou and Pingyao stream gauges are almost 1889 km^2 and 1406 km^2, respectively. As Fig. 2 shows, the forest in Tiaoxi watershed is the dominant land use type within the study area. Forest covers approximately 62 % of the land within the basin. Farmland, orchard, surface waters, and urban areas occupy the rest of catchment. Land use and land cover maps of Tiaoxi watershed were generated by the classification of digital orthophoto quadrangle and the survey data from State Bureau of Surveying and Mapping. The soil data was from the geological map (1 : 50 000 scale) developed by the second general survey of soil during the period of 1980 to 1985.

Soils of study area are dominated by the two Soil Groups: Red soils (46 %) and Paddy soils (27 %); other Soil Groups include Skeleton soils (10 %), Fluvio-aquic soils (5 %), Limestone soils (4 %), Yellow soils (3 %), and Purple soils (2 %) (Fig. 3). The name of each soil type and its properties are determined by the Second National Soil Survey of China and are shown in Tables S1 and S2.

2.2 TRMM data

TRMM provides global precipitation estimates from a wide variety of meteorological satellites (Huffman et al., 2010). Indeed, the TRMM estimates are available in the form of two products: a near real-time version (3B42RT) (about 6 h after real time) covering the global latitude belt from 60° N to 60° S and a gauge-adjusted post-real-time research version (3B42) (approximately 10–15 days after the end of each month) within the global latitude belt ranging between 50° N and 50° S. Both 3B42RT and 3B42 have 3 h temporal and 0.25° × 0.25° spatial resolutions. The 3B42RT uses the TRMM Combined Instrument (TCI) dataset, which includes the TRMM precipitation radar (PR) and

HESSD
12, 2497–2525, 2015

TRMM Microwave Imager (TMI), to calibrate precipitation estimates derived from available Low Earth Orbit (LEO) microwave (MW) radiometers. The 3B42RT then merges all of the estimates at 3 h intervals, and the gaps in the analyses are filled using Geostationary Earth Orbit (GEO) infrared (IR) data regionally calibrated based on the merged MW product. The 3B42 adjusts the monthly accumulations of the 3 h fields from 3B42RT based on a monthly gauge analysis, including the Global Precipitation Climatology Project (GPCP) (Arkin and Xie, 1994) $1^{\circ} \times 1^{\circ}$ monthly rain gauge analysis and the Climate Assessment and Monitoring System (CAMS) $0.5^{\circ} \times 0.5^{\circ}$ monthly rain gauge analysis (Shanhu Jiang, Liliang Ren, Yang Hong, Bin Yong, Xiaoli Yang, Fei Yuan, 2012). The daily satellite rainfall data employed in the current work are computed by aggregating 3 h temporal resolution data over 24 h for TRMM-3B42 product.

3 Methodology

3.1 Hydrological model

The Soil and Water Assessment Tool (SWAT) is a well-established, semi-distributed, eco-hydrologic model operating on daily, monthly or yearly time step. Main model components consist of weather, hydrology, soil temperature, plant growth, nutrients, pesticides, land management, bacteria and pathogens (Arnold and Fohrer, 2005; Arnold et al., 2012; Boorman, 2003; Hattermann et al., 2006; Manguerra and Engel, 1998).

Delineating watershed into subbasins and hydrologic response units (HRUs) needs three basic files: a digital elevation model (DEM), a land use and land cover (LULC) map, and a soil map. Topography was represented by a 30 m × 30 m elevation raster. Daily time-series of measured precipitation, air temperature, evaporation capacity and relative humidity were obtained from the six meteorological stations (Huzhou, Anji, Deqing, Changxing, Yuhang, and Linan).

In order to evaluate the quality of TRMM daily precipitation, correlation coefficient (CC), mean bias error (MBE), root mean square error (RMSE) and normalized root

HESSD
12, 2497–2525, 2015

mean square error (NRMSE) are calculated. As the root mean square error is an inappropriate measure for mean error and can be easily misinterpreted (Willmott and Matsuura, 2005), in this study, NRMSE and CC are mainly used to evaluate the accuracy of TRMM daily precipitation. For the NRMSE, the simulation is considered excellent if NRMSE < 10 %, good if 10–20 %, fair if 20–30 %, poor > 30 % (Jamieson et al., 1991; Signoretto and Plas, 2011).

3.2 Continuous evaluation indexes

3.2.1 Correlation coefficient

$$CC = \frac{\mathrm{cov}(P_{\mathrm{est}}, P_{\mathrm{obs}})}{\sigma(P_{\mathrm{est}}) \cdot \sigma(P_{\mathrm{obs}})}$$

where P_{est} and P_{obs} are respectively the gauge and satellite time series of rainfall data for a single position/pixel, cov (X, Y) is the empirical covariance between X and Y variables, and $\sigma(X)$ is the empirical SD of X.

3.2.2 Mean bias error

$$\mathrm{MBE}(\%) = \frac{\sum_{i=1}^{n} \left(P_{\mathrm{obs}}^{i} - P_{\mathrm{est}}^{i}\right)}{\sum_{i=1}^{n} P_{\mathrm{obs}}^{i}} \times 100$$

Where P_{obs}^{i} and P_{est}^{i} are respectively the precipitation value provided by gauge data and the precipitation estimation provided by a satellite product for a single position/pixel, at the ith time step with n being the number of considered time steps.

3.2.3 Root mean square error

$$\mathrm{RMSE} = \sqrt{\frac{\sum_{i=1}^{n} \left(P_{\mathrm{obs}}^{i} - P_{\mathrm{est}}^{i}\right)^{2}}{n}}$$

HESSD
12, 2497–2525, 2015

3.2.4 Normalized root mean square error

$$\mathrm{NRMSE}(\%) = \mathrm{RMSE} \Big/ \left(\frac{\sum_{i=1}^{n} P_{\mathrm{obs}}^{i}}{n} \right) \times 100$$

3.3 Categorical indexes

For the evaluation of the correspondence between the estimated and observed occurrence of rain events, several categorical verification statistics are also used in this study: probability of detection (POD), false alarm ratio (FAR) and critical success index (CSI). POD measures the fraction of observed events that were correctly diagnosed and is also called the hit rate. FAR provides the ratio of false alarm to total satellite-estimated events. CSI gives the overall fraction of events correctly diagnosed by the TRMM. Perfect values for these scores are POD = 1, FAR = 0, and CSI = 1.

3.3.1 Probability of detection

$$\mathrm{POD} = \frac{\sum_{i=1}^{n} I\left(P_{\mathrm{est}}^{i} > t | P_{\mathrm{obs}}^{i} > t\right)}{\sum_{i=1}^{n} I\left(P_{\mathrm{obs}}^{i} > t\right)}$$

Where t is a threshold value, and $I(a|b)$ is an indicator function indicating the number of occurrences where conditions a and b are respected.

The threshold value for categorical indexes t is fixed equal to 1.0 mm/24 h, according to Ebert et al. (2007). POD indicates the rainfall occurrences correctly detected by the considered estimation product. It is given by the ratio between the number of occurrences registered by both the reference and test data set and the occurrence registered only by the reference data set. POD is equal to 1 if the analyzed data set can represent all occurrences and 0 if no occurrences are detected.

HESSD
12, 2497–2525, 2015

3.3.2 False alarm ration

$$\mathrm{FAR} = \frac{\sum_{i=1}^{n} I\left(P_{\mathrm{est}}^{i} > t | P_{\mathrm{obs}}^{i} < t\right)}{\sum_{i=1}^{n} I\left(P_{\mathrm{est}}^{i} > t\right)}$$

Where FAR indicates the amount of rainfall occurrences detected by the considered estimation product when the reference data set is not indicating rainfall. It is equal to 0 if estimates do not reproduce any false occurrence and 1 if all registered occurrences do not correspond to observed data.

3.3.3 Critical success index

$$\mathrm{CSI} = \frac{\sum_{i=1}^{n} I\left(P_{\mathrm{est}}^{i} > t | P_{\mathrm{obs}}^{i} > t\right)}{\sum_{i=1}^{n} I\left(P_{\mathrm{est}}^{i} > t | P_{\mathrm{obs}}^{i} > t\right) + \sum_{i=1}^{n} I\left(P_{\mathrm{est}}^{i} < t | P_{\mathrm{obs}}^{i} > t\right) + \sum_{i=1}^{n} I\left(P_{\mathrm{est}}^{i} > t | P_{\mathrm{obs}}^{i} < t\right)}$$

Where CSI indicates the overall fraction of events that are correctly captured by the TRMM data. CSI is equal to 1 if the analyzed data can represent all occurrences and the estimates do not reproduce any false occurrence.

3.3.4 Hydrological model performance indexes

This study adopted two commonly used statistical criteria, the Nash–Sutcliffe Coefficient of Efficiency (NSCE) and the relative bias ratio, to evaluate the hydrological model performance (Meng et al., 2014). NSCE and BIAS are defined as:

$$\mathrm{NSCE} = \frac{\sum_{i=1}^{N}\left(Q_{i,\mathrm{o}} - \overline{Q}_{\mathrm{o}}\right)^2 - \sum_{i=1}^{N}\left(Q_{i,\mathrm{o}} - Q_{i,\mathrm{s}}\right)^2}{\sum_{i=1}^{N}\left(Q_{i,\mathrm{o}} - \overline{Q}_{\mathrm{o}}\right)^2}$$

$$\mathrm{BIAS} = \frac{\sum_{i=1}^{N} Q_{i,\mathrm{s}} - \sum_{i=1}^{N} Q_{i,\mathrm{o}}}{\sum_{i=1}^{N} Q_{i,\mathrm{o}}} \times 100\,\%$$

HESSD
12, 2497–2525, 2015

Where, $Q_{i,o}$ is the observed discharge of the ith day; $\overline{Q}_o$ is the average value of the observed discharge for the whole time; $Q_{i,s}$ is the simulated discharge of the ith day.

BIAS assesses the systematic errors of the simulated discharge, and NSCE is an indicator of model fit between the simulated and observed discharge. The highest skill level corresponds to NSCE = 1 and BIAS = 0 %. In addition, the determination coefficient (R^2) is used to measure the ability and reliability of the model in simulating the observed discharge.

4 Results and discussions

4.1 Comparison of TRMM rainfall with rain gauges data

Table 1 shows the statistics based on two types of rainfall datasets. Areal average rainfall is 2.9–5.0 mm d^{-1} for rain gauges and 3.1–5.2 mm d^{-1} for TRMM data in 1999–2008, respectively. While the difference is small, areal average rainfall based on TRMM is higher than that based on rain gauge data in most years except 2006 and 2008. A comparison of rainfall SDs calculated from the two data sets shows a greater difference than areal average rainfall. Maxim daily rainfall from rain gauge data is 56.1–121.6 mm d^{-1} in 1999–2008 and 64.4–124.0 mm d^{-1} for TRMM data in the same period.

Figure 4 shows the intensity distribution of daily rainfall and their contributions to the total rainfall as a function of rain rate in different years. It indicated that non-rainy days have the largest occurrence, and the second largest class was 0 < rainfall ≤ 3 mm, occurring about 20–30 % of the total days in gauges. Besides, the statistics for TRMM rainfall were different from gauge rainfall, the largest class was also non-rainy days, occurring about 65–75 % of total days, and the second largest class is 0 < rainfall ≤ 3 mm, occurring about 5–10 % of total days. That is to say more non-rainy days record in TRMM data and more days of light rain class (0 < rainfall ≤ 3 mm) in gauge data. That is because the TRMM data has a lower skill in correctly specifying moderate and

HESSD
12, 2497–2525, 2015

light rain rates on short time intervals (Michaelides et al., 2009), much light rainfall in some days are regarded as non-rainy in TRMM data. The sum of the first two classes, non-rainy and light rain classes, gives the similar percentage (80 %) for both TRMM data and gauge data. It can be calculated that although the occurrences of light rain (0 < rainfall ≤ 3 mm) are as high as 10–30 % of the total days, the contribution to the total rainfall amount is only about 1 % in both rainfall data.

It is important to point that although the high rainfall ranges occurs only about 1.1 % (maximal 2.4 % in 1999) of the total days, it plays a significant role in rainfall amount. The high rainfall class (> 50 mm) contributes to 16.3 % in average values (maximal 34.0 % in 1999) of the total rainfall for rain gauge data and 22.8 % (maximal 34.4 % in 1999) for TRMM data. For the class of 3–10 mm, both the occurrences and contribution rate of TRMM rainfall are smaller than those by gauge data, but the differences are small in every year. And in the range of 10–25 mm, the contribution rates are nearly equivalent between these two datasets. It is noted that TRMM data shows reasonable performances at annual scales. So it reproduces the surface observation-based histogram of precipitation.

The correlation coefficient (CC), probability of detection (POD), false alarm ratio (FAR), critical success index (CSI), and normalized root mean square error (NRMSE) are displayed at the different time aggregation.

Figure 5 shows the results of analyses at different time resolutions from one day to one month. Precipitation maps have been first temporally aggregated to the time resolution before evaluation analyses. Then, spatially averaged analyses for each time resolution were derived. A constant threshold value equal to 1.0 mm/24 h has been used to compute values. The values of indices on the daily scale, as CC = 0.57, POD = 0.60, and CSI = 0.46, are smaller than on the monthly scale, as CC = 0.87, POD = 0.94, and CSI = 0.92, in addition the indices of FAR and NRMSE are decreased from 0.34 and 265 to 0.02 and 40 with the increase of temporal resolution. The results underline that statistical indices describe an improvement of performances as time aggregation increases. And TRMM provides reasonable performance at monthly scales.

HESSD
12, 2497–2525, 2015

In order to further evaluate the relationships between the two data sets, the scatter plots of monthly TRMM rainfall against rain gauges rainfall data is shown in Fig. 6. The comparison was made for the five national meteorological stations and the areal average data of the nearest TRMM pixel. The results indicate very good linear relationship between the two rainfall datasets, with the determination coefficient (R^2) ranging from 0.79 to 0.90. The slope of the regression line ranges between 0.83 for Huzhou and 1.00 for Changxing, and 0.90 for areal average dataset. These values again indicate that the TRMM satellite tends to underestimate the monthly rainfall in this area. In general, the TRMM satellite is able to well capture the rainfall characterization well in comparison with the rainfall measurement from traditional rain gauges in different locations of the Tiaoxi watershed, although the systemic errors are also noted at monthly time step.

4.2 Hydrological processes simulation

To evaluate the runoff predictions by using the two rainfall datasets, experiment based on the SWAT model were conducted with input from by gauge rainfall and TRMM rainfall across the Tiaoxi watershed. SWAT contains parameters that need to be determined by using calibration. However, calibrated values are affected by correlations among parameters and observed data. For avoiding the effect of two dataset in calibration, the Nash–Sutcliffe efficiency index is used as the objective function, to evaluate hydrologic processes in two scenarios. The first scenario, the daily rain gauge rainfall was used to drive the model and optimize the parameter values, and then the daily TRMM rainfall was used to run the model with same parameter values, and the simulated runoffs in the two model runs were compared to each other. In the second scenario, the daily TRMM rainfall was used to drive the SWAT model and to optimize the parameter values, and then the rain gauge rainfall was used to drive the model. The result of parameters' optimization is shown in Table 2.

Table 3 shows the results of evaluation criteria of model performance. The model using conventional rain gauge data produced an overall good fit for hydrological processes in the first scenario. The relative runoff depth errors were lower than 2 %. In

HESSD
12, 2497–2525, 2015

addition, the relatively high values of R^2 (from 0.93 to 0.94) showed that the model described the variation of the observed streamflow well. Therefore, based on the presented results, the model was believed to be robust and provided a sound basis for testing the precision and applicability of TRMM rainfall. However, skill from the SWAT model by using the TRMM rainfall data is relatively lower. The E_{ns} values are not higher than 0.68 and the R^2 ranges from 0.75 to 0.84. In the second scenario, Table 3 shows that the TRMM rainfall-based model calibration had a slightly improved result with E_{ns} ranging between 0.51 and 0.70 and also increased R^2.

Figure 7 further compares the observed and simulated monthly runoff hydrographs from 1 January 2000 to 31 December 2008 based on TRMM rainfall estimate and rain gauges with their own optimal parameter values. It can be observed that the simulated streamflow hydrographs driven by rain gauge data exhibit a closer agreement with the observations than the model simulation using TRMM rainfall. Although extreme flow peaks tended to be underestimated in the model simulation with the TRMM rainfall, the results indicate that the TRMM rainfall data are still feasible for monthly stream flow simulation in this study area, According to Arnold et al. (2012), models are considered be very reliable if the monthly Nash–Sutcliffe efficiency index (NSE) is greater than 0.75. TRMM rainfall data has potential to be an alternative data source for the data-poor or ungauged basins, particularly in developing countries or remote locations.

4.3 Water balance

In addition to the comparison of streamflow hydrographs, water balance result is another important indicator for testing the validity of rainfall data (Xu et al., 2013). We examined the differences of water balance components from monthly streamflow simulations using rain gauges and TRMM rainfall. According to the above modeling results, comparison of the averaged water balance components from 2000 to 2008 is shown in Table 4. The model shows that the water balance partitions the precipitation into evaporation, transpiration, surface runoff and groundwater recharge (includes base flow).

HESSD
12, 2497–2525, 2015

In the rain gauge driven calculation, 49.0 % of precipitation were exhausted through evaporation and transpiration, while the rate is 50.2 % in TRMM rainfall data case. The groundwater recharge is 17.2 and 14.8 % respectively in gauge rainfall and TRMM rainfall case. Groundwater recharge is a large component and determines the amount of base flow. Although the volume of precipitation has a little difference (1268.0 and 1322.8 mm yr^{-1}), the estimated groundwater recharges are very similar (217.9 and 193.8 mm). In the case of total runoff, more precipitation is distributed into runoff in gauge rainfall case (527.1 mm) than in TRMM rainfall case (507.8 mm). In fact, this difference is mainly due to base flow estimation difference, which is 356.3 mm for gauge rainfall case, and 312.9 mm for TRMM rainfall case while the differences of runoff volume are small (170.8 and 194.9 mm).

5 Conclusions

The paper compares TRMM rainfall retrievals with rain gauge data and evaluates the TRMM rainfall as forcing data for hydrological applications and water balance analysis at the Tiaoxi catchment, China.

The results show that the differences of areal average rainfall calculated from two rainfall sources are small within an acceptable extent, but differences of the maximal daily and maximal 5 day rainfalls are large. So that the daily TRMM rainfall data are better at determining rain occurrences and mean values than at determining the rainfall extremes. Furthermore, the simulation of monthly hydrological processes shows that the SWAT model using both two types of data produces an overall good fit, but the statistical results indicate that the TRMM rainfall data are not suited for daily streamflow simulation in this area. The comparison of water balance components calculated by two types of rainfall shows that both data sources could describe the volume value of runoff and its compositions, which is very useful for watershed management.

The TRMM data as an example of the satellite-based rainfall products have great potential for applications in hydrological simulation and water balance calculations at

HESSD
12, 2497–2525, 2015

monthly or seasonal time steps. However, several shortcomings, such as the TRMM overestimates or underestimates in some years and areas cannot detect the extreme rainfall precisely, reducing the accuracy of streamflow simulation at short time steps and other applications including flood forecasting.

It is necessary to further develop algorithms of satellite-based rainfall estimation with combining different retrieval strategies in term of reaching better space–time resolutions and alleviating some of the deficiencies of single-sensor methods (Michaelides et al., 2009). And the extensive efforts of satellite based products evaluations are required in different climatic areas using different sensors and retrieval methods (Li et al., 2012). Moreover, as satellite-based rainfall data cover a great part of the world, we recommend an evaluation with global historical rainfall record (Matos et al., 2013). So that hydrologists and engineers could apply current generation satellite-based rainfall products for various purposes.

The Supplement related to this article is available online at doi:10.5194/hessd-12-2497-2015-supplement.

Acknowledgements. The authors thank Junjun Zhi and Miss Yao Zhu from CERS of Zhejiang University and Shenpan Lin from Michigan State University for their kind help and fruitful discussions regarding application of the SWAT model in China.

References

Arkin, P. and Xie, P.: The global precipitation climatology project: first algorithm intercomparison project, B. Am. Meteorol. Soc., 75, 401–419, doi:10.1175/1520-0477(1994)075<0401:TGPCPF>2.0.CO;2, 1994.

Arnold, J. G. and Fohrer, N.: SWAT2000: current capabilities and research opportunities in applied watershed modelling, Hydrol. Process., 19, 563–572, doi:10.1002/hyp.5611, 2005.

HESSD
12, 2497–2525, 2015

Arnold, J. G., Moriasi, D. N., Gassman, P. W., Abbaspour, K. C., White, M. J., Srinivasan, R., Santhi, C., Harmel, R. D., Van Griensven, A., and Van Liew, M. W.: SWAT: model use, calibration, and validation, Trans. Asabe, 55, 1491–1508, 2012.

Boorman, D.: Climate, Hydrochemistry and Economics of Surface-water Systems (CHESS): adding a European dimension to the catchment modelling experience developed under LOIS, Sci. Total Environ., 314–316, 411–437, doi:10.1016/S0048-9697(03)00066-4, 2003.

Chappell, A., Renzullo, L. J. L., Raupach, T. T. H., and Haylock, M.: Evaluating geostatistical methods of blending satellite and gauge data to estimate near real-time daily rainfall for Australia, J. Hydrol., 493, 105–114, doi:10.1016/j.jhydrol.2013.04.024, 2013.

Dinku, T., Chidzambwa, S., Ceccato, P., Connor, S. J., and Ropelewski, C. F.: Validation of high-resolution satellite rainfall products over complex terrain, Int. J. Remote Sens., 29, 4097–4110, doi:10.1080/01431160701772526, 2008.

Ebert, E., Janowiak, J., and Kidd, C.: Comparison of near-real-time precipitation estimates from satellite observations and numerical models, Bull. Am. Meteorol. Soc., 88, 47–64, doi:10.1175/BAMS-88-1-47, 2007.

Hattermann, F. F., Krysanova, V., Habeck, A., and Bronstert, A.: Integrating wetlands and riparian zones in river basin modelling, Ecol. Modell., 199, 379–392, doi:10.1016/j.ecolmodel.2005.06.012, 2006.

Hu, Q., Yang, D., Wang, Y., and Yang, H.: Accuracy and spatio-temporal variation of high resolution satellite rainfall estimate over the Ganjiang River Basin, Sci. China Technol. Sci., 56, 853–865, doi:10.1007/s11431-013-5176-7, 2013.

Huffman, G., Adler, R., Bolvin, D., and Nelkin, E.: The TRMM multi-satellite precipitation analysis (TMPA), in: Satellite rainfall applications for surface hydrology, edited by: Gebremichael, M. and Hossain, F., Springer, Dordrecht, the Netherland, 3–22, 2010.

Hunink, J. E., Immerzeel, W. W., and Droogers, P.: A High-resolution Precipitation 2-step mapping Procedure (HiP2P): development and application to a tropical mountainous area, Remote Sens. Environ., 140, 179–188, doi:10.1016/j.rse.2013.08.036, 2014.

Jamieson, P. D., Porter, J. R., and Wilson, D. R.: A test of the computer simulation model ARCWHEAT1 on wheat crops grown in New Zealand, F. Crop. Res., 27, 337–350, doi:10.1016/0378-4290(91)90040-3, 1991.

Jiang, S., Ren, L., and Yong, B.: Evaluation of high-resolution satellite precipitation products with surface rain gauge observations from Laohahe Basin in northern China, Water Sci. Eng., 3, 405–417, doi:10.3882/j.issn.1674-2370.2010.04.004, 2010.

HESSD
12, 2497–2525, 2015

Jiang, S., Ren, L., Hong, Y., Yong, B., Yang, X., Yuan, F., and Ma, M.: Comprehensive evaluation of multi-satellite precipitation products with a dense rain gauge network and optimally merging their simulated hydrological flows using the Bayesian model averaging method, J. Hydrol., 452–453, 213–225, doi:10.1016/j.jhydrol.2012.05.055, 2012.

Kummerow, C.: Beamfilling errors in passive microwave rainfall retrievals Christian Kummerow, J. Appl. Meteorol., 37, 356–370, doi:10.1175/1520-0450(1998)037<0356:BEIPMR>2.0.CO;2, 1998.

Li, X.-H. X., Zhang, Q., and Xu, C. C.-Y.: Suitability of the TRMM satellite rainfalls in driving a distributed hydrological model for water balance computations in Xinjiang catchment, Poyang lake basin, J. Hydrol., 426–427, 28–38, doi:10.1016/j.jhydrol.2012.01.013, 2012.

Manguerra, H. B. and Engel, B. A.: Hydrologic parameterization of watersheds for runoff prediction using SWAT, J. Am. Water Resour. Assoc., 34, 1149–1162, doi:10.1111/j.1752-1688.1998.tb04161.x, 1998.

Masih, I., Maskey, S., Uhlenbrook, S., and Smakhtin, V.: Assessing the impact of areal precipitation input on streamflow simulations using the SWAT model1, JAWRA J. Am. Water Resour. Assoc., 47, 179–195, doi:10.1111/j.1752-1688.2010.00502.x, 2011.

Matos, J. P., Cohen Liechti, T., Juízo, D., Portela, M. M., and Schleiss, A. J.: Can satellite based pattern-oriented memory improve the interpolation of sparse historical rainfall records?, J. Hydrol., 492, 102–116, doi:10.1016/j.jhydrol.2013.04.014, 2013.

Meng, J., Li, L., Hao, Z., Wang, J., and Shao, Q.: Suitability of TRMM satellite rainfall in driving a distributed hydrological model in the source region of Yellow River, J. Hydrol., 509, 320–332, doi:10.1016/j.jhydrol.2013.11.049, 2014.

Michaelides, S., Levizzani, V., Anagnostou, E., Bauer, P., Kasparis, T., and Lane, J. E.: Precipitation: measurement, remote sensing, climatology and modeling, Atmos. Res., 94, 512–533, doi:10.1016/j.atmosres.2009.08.017, 2009.

Moreno, H. A., Vivoni, E. R., and Gochis, D. J.: Utility of quantitative precipitation estimates for high resolution hydrologic forecasts in mountain watersheds of the Colorado Front Range, J. Hydrol., 438–439, 66–83, doi:10.1016/j.jhydrol.2012.03.019, 2012.

Ochoa, A., Pineda, L., Crespo, P., and Willems, P.: Evaluation of TRMM 3B42 precipitation estimates and WRF retrospective precipitation simulation over the Pacific–Andean region of Ecuador and Peru, Hydrol. Earth Syst. Sci., 18, 3179–3193, doi:10.5194/hess-18-3179-2014, 2014.

HESSD
12, 2497–2525, 2015

Shen, Y., Xiong, A., Wang, Y., and Xie, P.: Performance of high-resolution satellite precipitation products over China, J. Geophys. Res. Atmos., 115, 2156–2202, doi:10.1029/2009JD012097, 2010.

Signoretto, M. and van de Plas, R.: Tensor versus matrix completion: a comparison with application to spectral data, Signal Process. Lett. IEEE, 18, 403–406, doi:10.1109/LSP.2011.2151856, 2011.

Stampoulis, D. and Anagnostou, E. E. N.: Evaluation of global satellite rainfall products over Continental Europe, J. Hydrometeorol., 13, 588–603, doi:10.1175/JHM-D-11-086.1, 2012.

Tian, Y. and Peters-Lidard, C. D.: A global map of uncertainties in satellite-based precipitation measurements, Geophys. Res. Lett., 37, L24407, doi:10.1029/2010GL046008, 2010.

Ud din, S., Al-Dousari, A., Ramdan, A., and Al Ghadban, A.: Site-specific precipitation estimate from TRMM data using bilinear weighted interpolation technique: an example from Kuwait, J. Arid Environ., 72, 1320–1328, doi:10.1016/j.jaridenv.2007.12.013, 2008.

Wilk, J., Kniveton, D., Andersson, L., Layberry, R., Todd, M. C., Hughes, D., Ringrose, S., and Vanderpost, C.: Estimating rainfall and water balance over the Okavango River Basin for hydrological applications, J. Hydrol., 331, 18–29, doi:10.1016/j.jhydrol.2006.04.049, 2006.

Willmott, C. and Matsuura, K.: Advantages of the mean absolute error (MAE) over the root mean square error (RMSE) in assessing average model performance, Clim. Res., 30, 79–82, doi:10.3354/cr030079, 2005.

Worqlul, A. W., Maathuis, B., Adem, A. A., Demissie, S. S., Langan, S., and Steenhuis, T. S.: Comparison of rainfall estimations by TRMM 3B42, MPEG and CFSR with ground-observed data for the Lake Tana basin in Ethiopia, Hydrol. Earth Syst. Sci., 18, 4871–4881, doi:10.5194/hess-18-4871-2014, 2014.

Xu, H., Xu, C.-Y., Chen, H., Zhang, Z., and Li, L.: Assessing the influence of rain gauge density and distribution on hydrological model performance in a humid region of China, J. Hydrol., 505, 1–12, doi:10.1016/j.jhydrol.2013.09.004, 2013.

Yan, J. and Gebremichael, M.: Estimating actual rainfall from satellite rainfall products, Atmos. Res., 92, 481–488, doi:10.1016/j.atmosres.2009.02.004, 2009.

Zhang, W., Yan, Y., Zheng, J., and Li, L.: Temporal and spatial variability of annual extreme water level in the Pearl River Delta region, China, Glob. Planet. Change, 69, 35–47, doi:10.1016/j.gloplacha.2009.07.003, 2009.

HESSD
12, 2497–2525, 2015

Table 1. Comparison of statistical indexes between areal averaged TRMM rainfall and rain gauges rainfall.

Year	Areal average ($mm\,d^{-1}$)		SD (mm)		Max. daily rainfall ($mm\,d^{-1}$)		Max. 5 day rainfall (mm/5 d)	
	Gauging	TRMM	Gauging	TRMM	Gauging	TRMM	Gauging	TRMM
1999	5.0	5.2	173.3	185.9	98.0	106.6	396.0	408.4
2000	3.1	3.5	61.7	86.7	57.9	76.2	235.5	275.7
2001	3.8	4.1	102.7	142.8	96.9	108.3	324.0	380.2
2002	4.1	4.5	70.3	163.3	56.1	124.0	220.5	398.0
2003	2.9	3.1	50.6	77.7	59.1	67.6	207.2	274.1
2004	3.1	3.2	66.1	79.0	80.1	76.9	236.8	272.6
2005	3.1	3.6	74.7	118.6	81.3	98.9	284.5	346.3
2006	3.3	3.2	76.9	67.3	73.9	64.4	265.6	233.2
2007	3.4	3.6	116.3	124.0	121.6	105.0	348.9	368.9
2008	4.2	3.8	130.3	116.9	101.2	93.4	362.9	345.3
Average	3.6	3.8	92.3	116.2	82.6	92.1	288.2	330.3

HESSD
12, 2497–2525, 2015

Table 2. Sensitivity analysis results for hydrologic parameters.

Parameter	Description	Lower bound	Upper bound	Rank	*T* Stat	*P* value	Optimal value		Process
							Scenario 1	Scenario 2	
CN2*	Initial SCS runoff curve number for moisture condition II	−0.2	0.2	1	9.14	3.47E−19	0.19	0.16	Runoff
GW_DELAY	Groundwater delay time (days)	30	350	2	−5.62	2.46E−08	55.56	206.52	Groundwater
CH_N2	Manning's "*n*" value for the main channel.	0.01	0.3	3	−5.32	1.26E−07	0.03	0.11	Runoff
ALPHA_BF	Baseflow alpha factor-Baseflow recession constant	0.01	1	4	5.15	3.07E−07	0.68	0.80	Runoff
SOL_AWC*	Available water capacity of the soil layer ($mm\,H_2O\,mm^{-1}$ soil)	−0.8	0.8	5	4.91	1.06E−06	0.42	0.51	Soil
CH_K2	Effective hydraulic conductivity in main channel alluvium ($mm\,h^{-1}$)	0	500	6	−4.06	5.23E−05	134.84	144.63	Channel
ESCO	Soil evaporation compensation factor	0.01	1	7	−2.17	3.00E−02	0.87	0.72	Evaporation
GW_REVAP	Groundwater "revap" coefficient	0.02	0.2	8	2.16	3.09E−02	0.12	0.18	Groundwater
EPCO	Plant uptake compensation factor	0.01	1	9	1.48	1.39E−01	0.63	0.65	Evaporation
Revapmn	Threshold depth of water in the shallow aquifer for "revap" to occur (mm)	0	500	10	1.29	1.98E−01	332.53	233.25	Groundwater
Surlag	Surface runoff lag time.	0.05	24	11	0.92	3.60E−01	5.85	6.10	Runoff
Sol_K*	Saturated hydraulic conductivity	−0.2	0.2	12	0.91	3.64E−01	0.07	0.12	Soil

HESSD
12, 2497–2525, 2015

Table 3. Statistics index for the model of the Tiaoxi river basin using SWAT.

Scenario	Station	Gauge Rainfall-based model			TRMM Rainfall-based model		
		E_{ns}	DE	R^2	E_{ns}	DE	R^2
First	Gangkou	0.86	−0.02	0.93	0.50	0.06	0.75
	Pingyao	0.86	0.01	0.94	0.68	0.18	0.84
Second	Gangkou	0.81	−0.12	0.91	0.51	−0.05	0.73
	Pingyao	0.83	−0.05	0.94	0.70	0.08	0.85

HESSD
12, 2497–2525, 2015

Table 4. Components Gauge-based model TRMM-based model.

Components	Gauge-based model			TRMM-based model		
	Volume ($mm\,yr^{-1}$)	Percentage of precipitation (%)	Percentage of total runoff (%)	Volume ($mm\,yr^{-1}$)	Percentage of precipitation (%)	Percentage of total runoff (%)
Precipitation	1268.0			1312.8		
Evaporation and transpiration	621.9	49.0		659.4	50.2	
Groundwater recharge	217.9	17.2		193.8	14.8	
Total runoff	527.1	41.6		507.8	38.7	
Surface runoff	170.8	13.5	32.4	194.9	14.8	38.4
Base flow	356.3	28.1	67.6	312.9	23.8	61.6

HESSD
12, 2497–2525, 2015

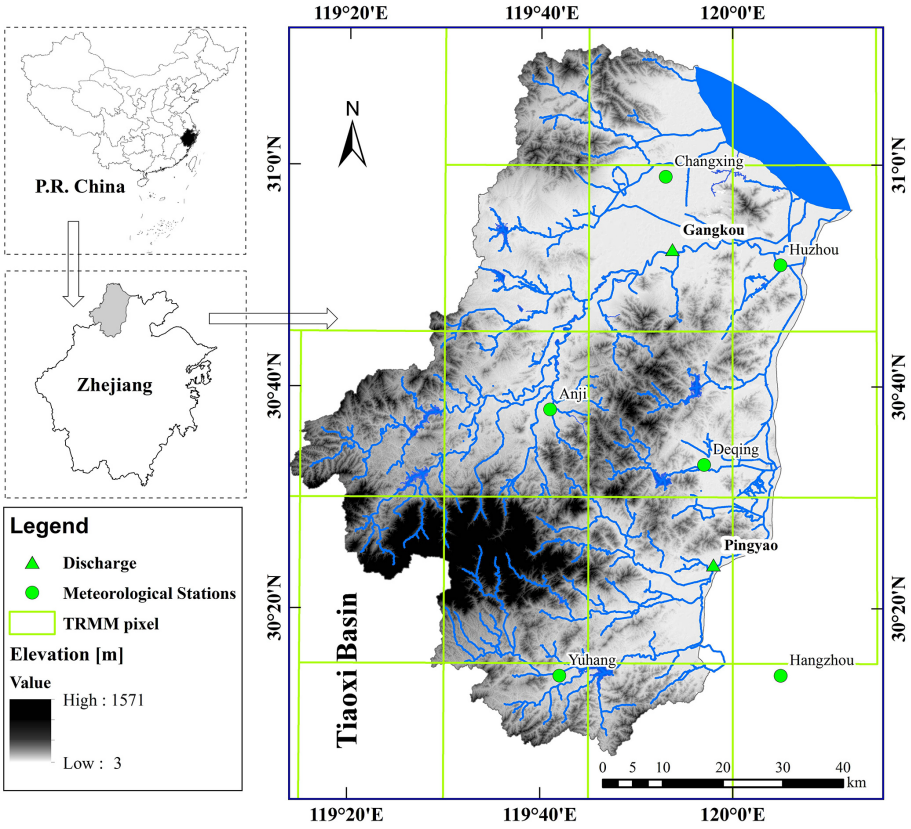

Figure 1. Location of Tiaoxi catchment in Taihu Lake basin and the distribution of stations.

HESSD
12, 2497–2525, 2015

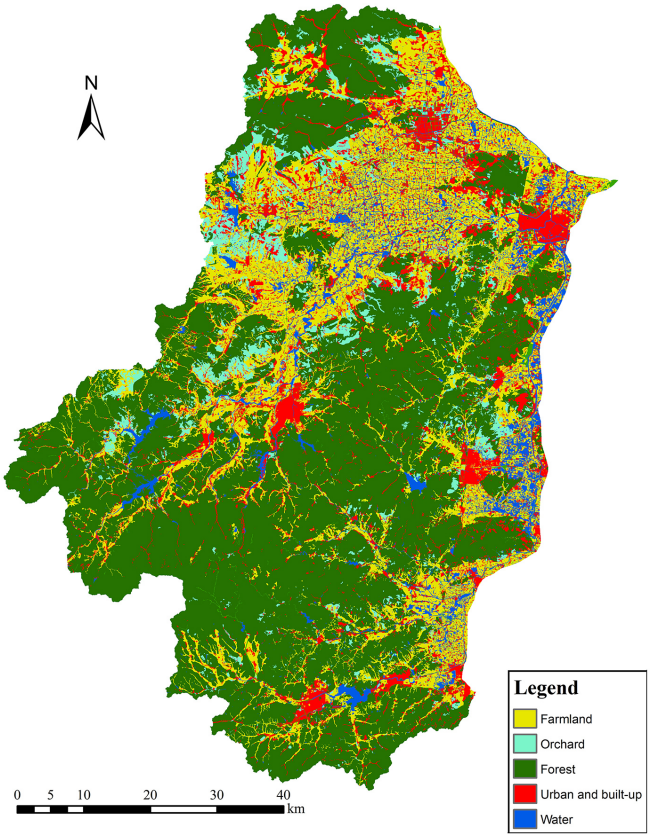

Figure 2. The land use map of study area.

HESSD
12, 2497–2525, 2015

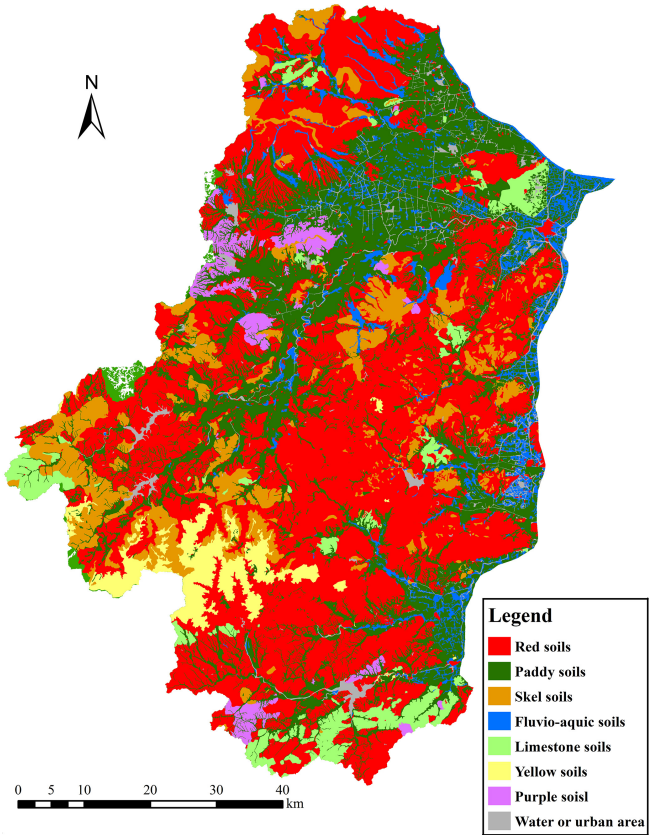

Figure 3. The soil type map of study area.

HESSD
12, 2497–2525, 2015

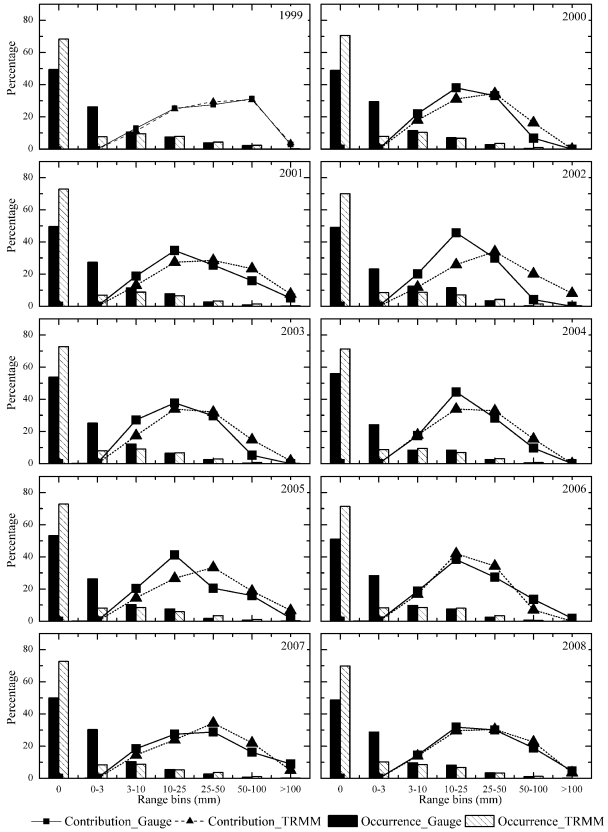

Figure 4. Distribution of daily rainfall in different rainfall classes and their relative contributions to the total rainfall in different years.

HESSD
12, 2497–2525, 2015

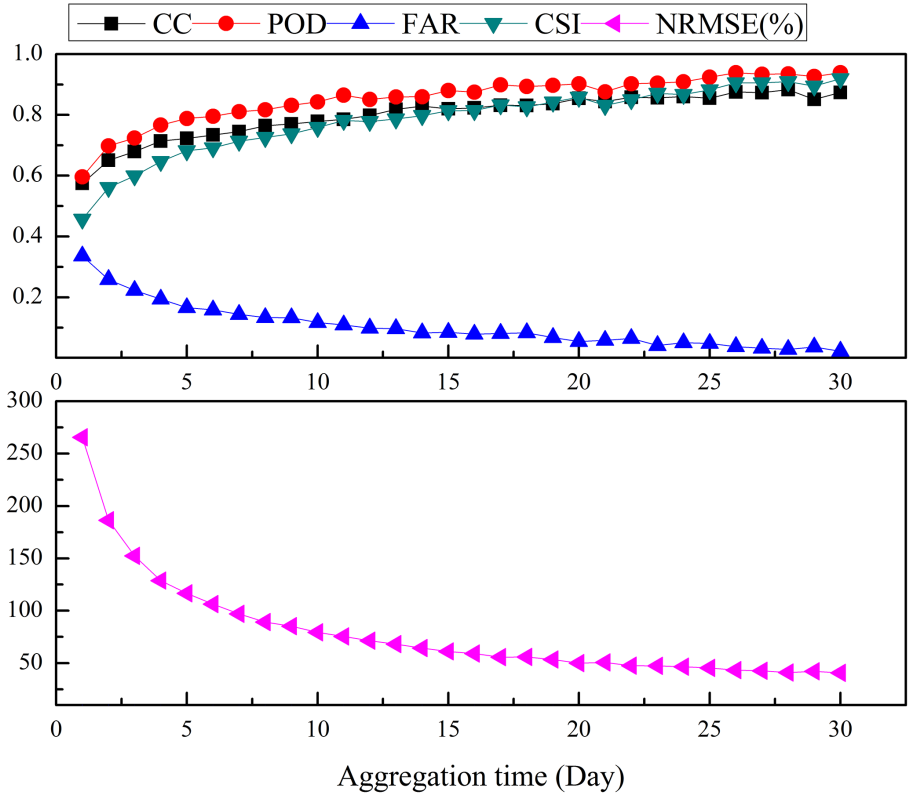

Figure 5. The evaluation of the TRMM detection using performance-indices.

HESSD
12, 2497–2525, 2015

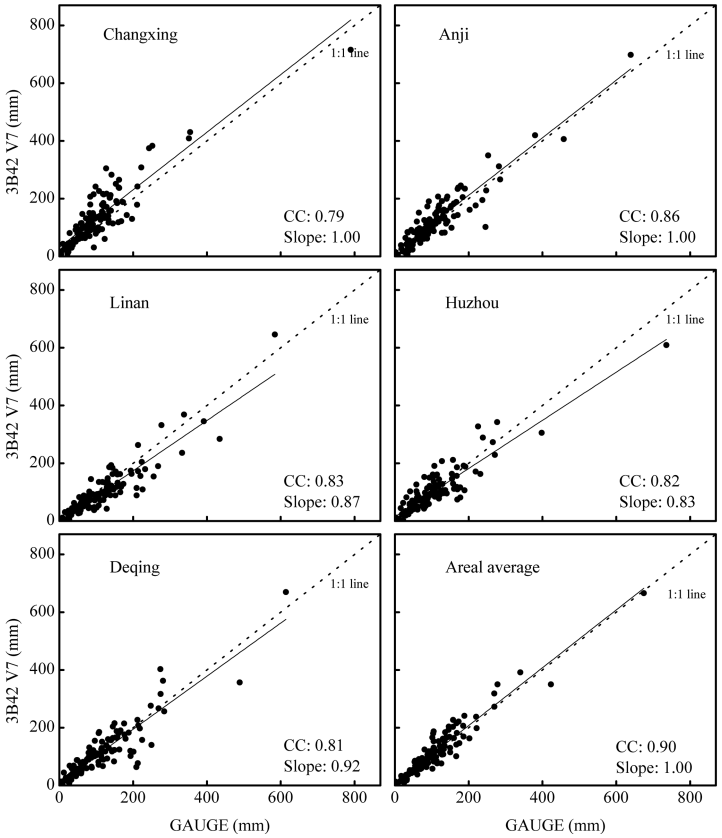

Figure 6. Scatter plots of monthly rainfall from Tropical Rainfall Measuring Mission (TRMM) and rain gauges data for the national meteorological stations and the areal average data.

HESSD
12, 2497–2525, 2015

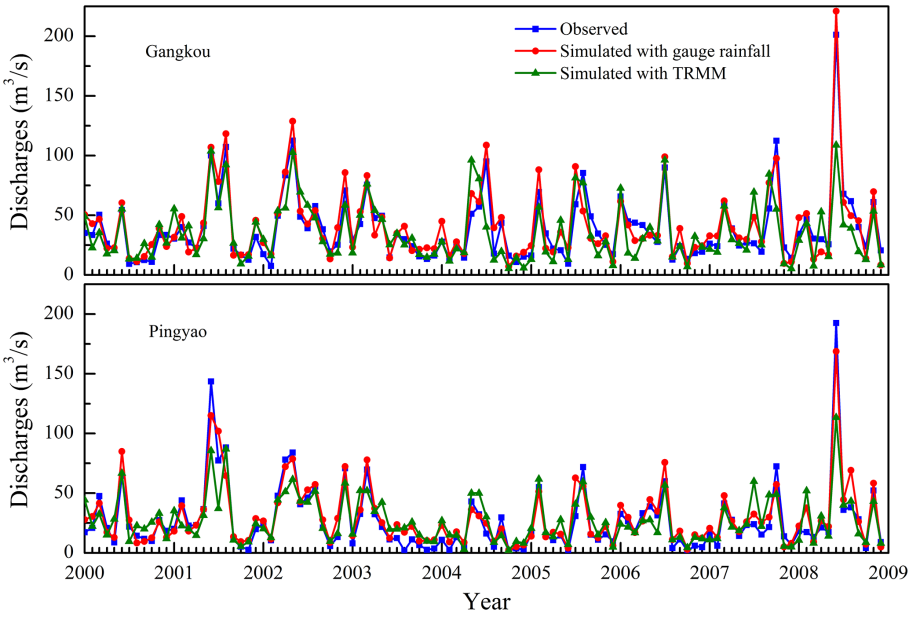

Figure 7. Comparison of the observed and simulated monthly hydrographs at Gangkou and Pingyao stations.

HESSD
12, 2497–2525, 2015